A novel optical investigation technique for railroad track inspection and assessment

Alessandro Sabato*, Christopher H. Beale, Christopher Niezrecki
University of Massachusetts Lowell, 1 University Avenue, Lowell, MA, USA 01852

ABSTRACT

Track failures due to cross tie degradation or loss in ballast support may result in a number of problems ranging from simple service interruptions to derailments. Structural Health Monitoring (SHM) of railway track is important for safety reasons and to reduce downtime and maintenance costs. For this reason, novel and cost-effective track inspection technologies for assessing tracks' health are currently insufficient and needed. Advancements achieved in recent years in cameras technology, optical sensors, and image-processing algorithms have made machine vision, Structure from Motion (SfM), and three-dimensional (3D) Digital Image Correlation (DIC) systems extremely appealing techniques for extracting structural deformations and geometry profiles. Therefore, optically based, non-contact measurement techniques may be used for assessing surface defects, rail and tie deflection profiles, and ballast condition. In this study, the design of two camera-based measurement systems is proposed for crossties-ballast condition assessment and track examination purposes. The first one consists of four pairs of cameras installed on the underside of a rail car to detect the induced deformation and displacement on the whole length of the track's cross tie using 3D DIC measurement techniques. The second consists of another set of cameras using SfM techniques for obtaining a 3D rendering of the infrastructure from a series of two-dimensional (2D) images to evaluate the state of the track qualitatively. The feasibility of the proposed optical systems is evaluated through extensive laboratory tests, demonstrating their ability to measure parameters of interest (e.g. crosstie's full-field displacement, vertical deflection, shape, etc.) for assessment and SHM of railroad track.

Keywords: Ballast, crosstie, Digital Image Correlation, railroad, Structure from Motion, Structural Health Monitoring

1. INTRODUCTION

The 2013 Report Card for America's Infrastructure released by the American Society of Civil Engineering (ASCE) rated the state of the U.S. railroads as mediocre [1]. Statistic released by the Federal Railroad Administration (FRA) for the decade 2005 – 2015, showed that one-out-of-three of the nearly 25,000 accidents happened nationwide were caused by track failures at different levels (i.e. rails, crossties, joint bars, anchor, etc.) [2].

Railways include several parts such as rails, crossties (or sleepers), fasteners, ballast, and an underlying subgrade, each of them with different functionalities. An acceptable state of health of each part prevents the onset of potentially dangerous situations, which may lead to train derailments. For instance, the absence or failure of fastening systems can lead to unwanted displacements of the rail, which may cause accidents similar to the freight train derailment that occurred in 2016 at Mosier, OR [3]. Train derailment can also occur when the support of the ballast under the crosstie becomes concentrated rather than being uniformly distributed. This failure mechanism, known as center binding, is generated by different levels of abrasion experienced by the crosstie-ballast system at different locations as encountered in 2013 when a freight train derailed in Bronx, NY [4]. Structural Health Monitoring (SHM) of railway tracks is important to reduce risks, downtime, and maintenance costs. As a result, novel and cost-effective track inspection technologies for assessing tracks' health are currently needed.

To improve the quality of railroad track health monitoring data, several measurement techniques have been implemented. Sensing methods using accelerometers [5], strain gauges [5], optical Fiber Bragg Grating (FBG) strain sensors [6], impedance-based damage techniques [7], and Wireless Sensor Networks (WSNs) [8] have been proposed in the past. Nevertheless, contact-type systems are labor intensive, time consuming, and can be used for obtaining information at a few discrete points only. For this reason, recent technological developments have made non-contact measurements such as active and passive infrared (IR) images [9], Ultrasonic Testing (UT) [10], and Ground Penetrating Radar (GPR) [11], extremely appealing, but still expensive tools for railroad tracks SHM. Advancements achieved in recent years in cameras technology, optical sensors, image-processing algorithms, and machine vision techniques made Structure from

*Alessandro_Sabato@uml.edu; phone +1 (978) 934-5253

Motion (SfM) [12], and three-dimensional (3D) Digital Image Correlation (DIC) systems [13] effective methods for extracting structural deformations, geometry profiles, and to detect potentially dangerous situations at an early stage, while not interfering with the structure operations.

In this paper, the preliminary design of a novel railroad tracks examination system that detects crossties' vertical deflection and full field displacement using 3D-DIC techniques is described. It consists of four pairs of cameras installed on the underside of a rail car to detect the induced displacements on the whole length of the crosstie. An evaluation of the performance of the system is provided together with details for improving the quality of the performed measurements. Furthermore, another optical-based system using SfM and range imaging algorithms is introduced with the purpose to qualitatively asses the state of the track by creating a 3D rendering of the infrastructure from a set of two-dimensional (2D) images. If fully developed, the proposed systems would enable track inspectors to perform more frequent and cost-effective measurements of tracks, assess the conditions of the crosstie-ballast interface without contacting the infrastructure, and permit interrogation while trains are moving at typical operating speeds (e.g. 60 mph).

2. CROSSTIES ASSESSMENT USING THE 3D DIC SYSTEM

Within this work, the possibility to develop a 3D DIC system to monitor the crosstie deflection profile over its entire length is investigated. For this purpose, a wooden full-scale model of a railroad track has been built and instrumented. The dimensions of the model are equivalent to those of a real railroad and are shown in Figure 1. The only difference consists of the crossties thickness (i.e. 0.019 m), which is considerably smaller than that of a real-world tie (i.e. 0.178 m). Thinner ties were used for the purpose of producing the vertical deflection characterizing real-world ties (i.e. displacement ranging from $1 \cdot 10^{-3}$ to $8 \cdot 10^{-3}$ m) without applying loads on the order of 10^2 kN (nearly 22,500 lbf) [14].

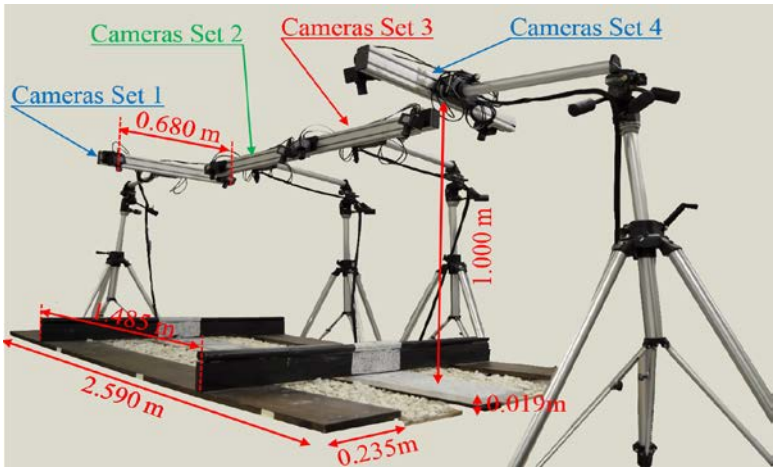

Figure 1. Mock-test experimental setup and dimensions.

As shown in Figure 1, each camera set consists of a pair of 2 Megapixel FWX201 series digital cameras manufactured by Baumer GmBH. Each camera has a resolution equal to 1626 x 1236 pixels, a pixel size of (4.4 x 4.4) 10^{-6} m, and installed with 8.5 mm focal length lenses. It is noted that only one pair of cameras was available and used during the tests. The four pairs depicted in Figure 1 serve as conceptual setup of the proposed design. Because of geometrical limitations due to the features of the train cars commonly used (i.e. maximum space available underneath the train cars), the 3D DIC system was positioned to have a working distance of 1 meter, a 36.5° separation angle, and a base distance of 0.68 m. In this configuration, the stereo-photogrammetry system allowed for measuring a limited area of 0.81 x 0.67 m, corresponding to nearly 56% of the distance between the rails. Since a single system cannot cover the whole length of the crosstie, the full field of view (FOV) has been obtained by stitching together the images recorded using the cameras placed at four different positions [15], in a setup similar to that shown in Figure 2. In order to combine the individual sections into a single image, the recorded FOVs were laid out with several centimeters of overlap and a series of three targets were used as reference between two adjacent images. Since only one pair of cameras was available during the

tests, the camera pair was repositioned around the model to account for all the camera sets presented in the conceptual setup.

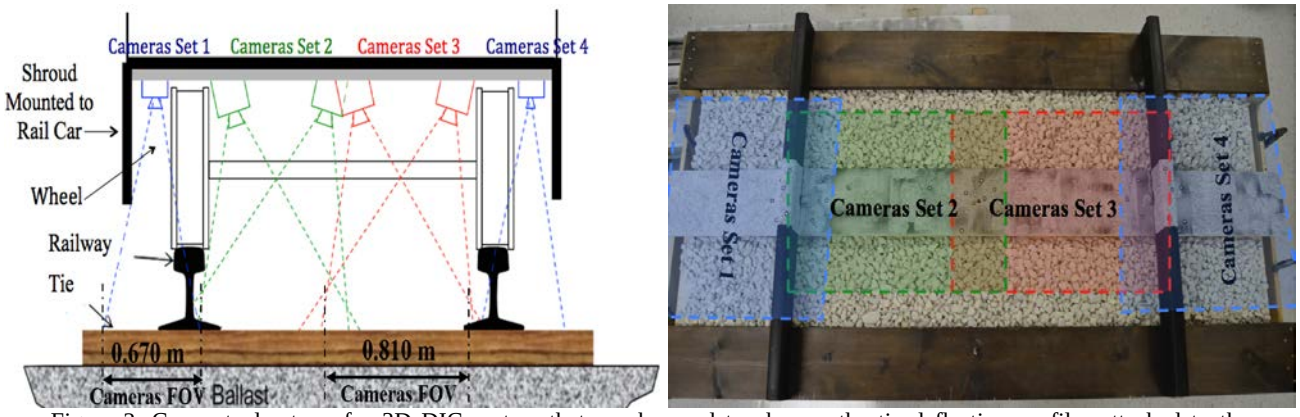

Figure 2. Conceptual setup of a 3D DIC system that can be used to observe the tie deflection profiles attached to the underside of a rail car (left) and cameras sets' FOVs for the adopted configuration (right) (pictures not to scale).

To measure the performance of the proposed system, different center binding conditions were simulated on the middle tie of the setup shown in Figure 1 and measurements were recorded as different loading conditions were applied. In particular, zero and 510 N (114.65 lbf) loads were applied to the crosstie to simulate the effects of the transit of a train. The center binding occurs as the support of ballast under the crosstie, initially uniformly distributed, is concentrated at the rail-seat. As a result, the ballast provides a firm support at the crosstie' s center only, while it cantilevers at its free edges. This condition was simulated providing localized support in specific areas only, by placing a support underneath the crosstie being tested as shown in Figure 3.

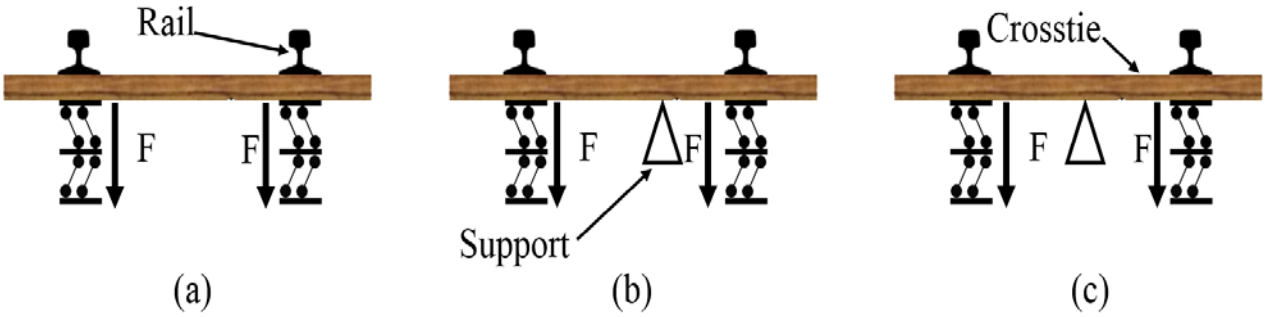

Figure 3. Center binding conditions simulated during the performed experiments (not to scale): (a) uniform support, (b) supported at one-quarter of the distance from the right rail, (c) supported in the middle of the distance between the rails.

The tests performed aimed to measure and compare the out-of-plane displacement (i.e. vertical displacement Z) and deformation of the tie's longitudinal profile when the load was present compared to when the load was absent. For each of the two loading conditions, five snapshots were taken to allow data averaging during post-processing analyses and to prove measurements repeatability. The setup parameters used in the analysis are summarized in Table 1. It should be noticed that the first five images recorded in each test refer to the unloaded condition and were used to evaluate the measurement's noise floor. An analysis of the noise floor is fundamental as it allows gaining general information on the minimum displacement detectable by the system and provides a first understanding about the quality of the expected results. The upper and lower values of the noise floor range of the recorded images were evaluated before and after the stages were stitched together using the SVIEW^{TM} software, developed by the German company GOM [16, 17]. The results obtained are summarized in Table 2 for a comparison at a glance.

Table 1. Setup parameters used for compute the displacements.

Facets		Filtering		Computational Parameters		Deviation	
Size (pixel)	17 x 17	Type (-)	Median	Accuracy (-)	0.040	Calibration (pixel)	0.026
Step (pixel)	15 x 15	Run (-)	5	Residual (-)	20.000	Scale (mm)	0.006
Dots dimension (mm)	3	Size (-)	3	Angle variance (°)	-32.8/45.1	Intersection (-)	0.300

Table 2. Measured out-of-plane displacement noise floor before and after the stitching operation.

	Before Stitching			After Stitching		
	Condition (a)	Condition (b)	Condition (c)	Condition (a)	Condition (b)	Condition (c)
Zmax (mm)	0.0103	0.0093	0.0112	0.1697	0.1371	0.1311
Zmin (mm)	-0.0059	-0.0069	-0.0046	-0.1689	-0.1944	-0.1502
ΔZ (mm)	0.0162	0.0163	0.0158	0.0867	0.1106	0.0845

Data reported have been obtained by averaging the noise floor of the first five images recorded for each of the four cameras position considered and for each of the three simulated center binding conditions. As observed in Table 2, the system is capable of detecting displacements on the order of $1.61 \cdot 10^{-5}$ and $3.17 \cdot 10^{-4}$ m as the images are considered solely and stitched together respectively. An increase in the measurement's noise floor is normal as several FOVs are stitched together for creating a wider one. Additionally, differences can be attributed to the uncertainty of manually relocating the camera pair in each orientation during the experiment. Nevertheless, the accuracy of the measurement is still good enough to allow for detection of the typical vertical deflection characterizing real-world ties in normal operational conditions.

The 3D DIC system has been employed to measure the full-field vertical displacement Z experienced by the tie as the 510 N load is applied. Figure 4 presents the full-field out-of-plane vertical displacement measured in false colors superimposed on an image of the lab-scale model and the crosstie's longitudinal profile for the three different simulated ballast conditions. Different longitudinal profiles correspond to different supporting conditions.

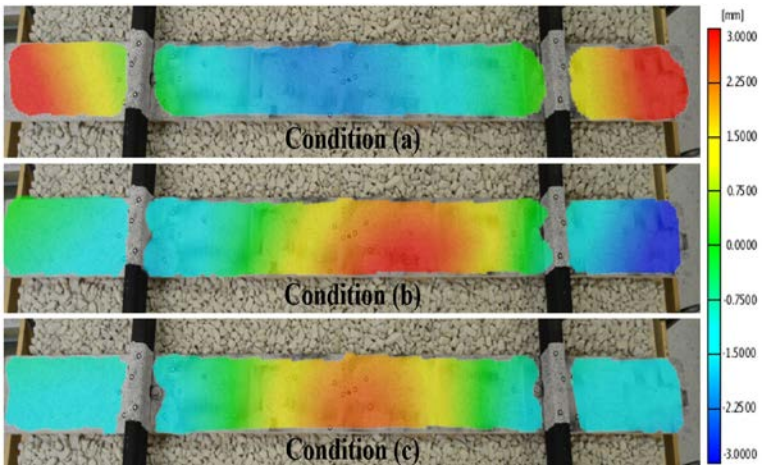

Figure 4. Out-of-plane vertical displacement for the three boundary conditions (a), (b), and (c) described in Figure 3 and a 510 N load applied to the rail superimposed on an image of the model.

The results show how the 3D DIC system is capable of highlighting these differences easily. In general, it is observed that the presence of a support induces a positive (upward) displacement of the crosstie at the location of the support. In contrast, the absence of the localized support resulted in a negative displacement resembling the deflection of a simply

supported cantilever beam. As shown in Figure 5, when the crosstie is evenly supported (condition (a)), a fairly uniform deflection is observed in the portion between the rails.

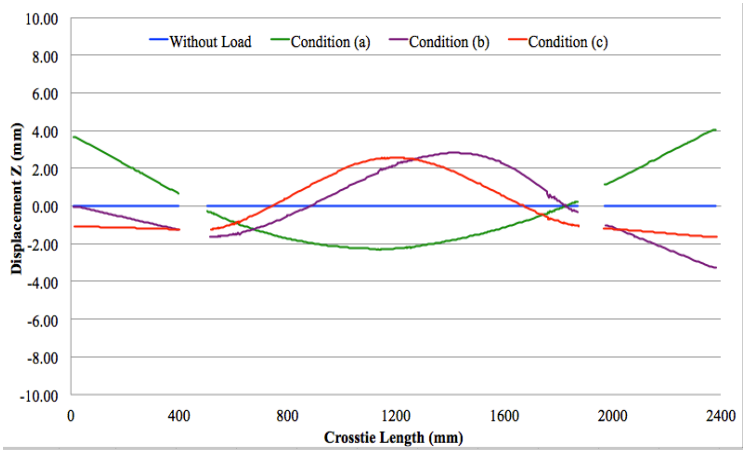

Figure 5. Tie longitudinal profiles for the three boundary conditions (a), (b), and (c) described in Figure 3 and a 510 N load applied to the rail.

The profile is parabolic with the lower vertex equal to $-2.31 \cdot 10^{-3}$ m in correspondence with the crosstie's middle point. When the support is located in a specific area between the rails, the crosstie rises close to the support and negative displacements are observed at the free edges. This is verified by the rightmost plot of Figure 4. The displacements at the support locations are $2.58 \cdot 10^{-3}$ and $2.82 \cdot 10^{-3}$ m for conditions (c) and (b) respectively. The displacements at the free edges are within the range of $-1.64 \cdot 10^{-3}$ and $-3.29 \cdot 10^{-3}$ m.

2.1 Evaluation of vibrations on the DIC measurements' accuracy

Strong motions and high levels of vibration characterize railroad service environments. Therefore, the possibility for an optical-based measurement technique to yield the predicted accuracy as the system is placed underneath a moving train car is of concern. For this reason, a method of compensation for vibration has been added to the 3D DIC system described in the previous paragraph. The isolation system has been designed so that:

- Vibrations transmitted from the train to the cameras were reduced;
- Only low frequency rigid-body-type motions could be transmitted, so they can be removed using suitable post-processing algorithms [16, 17].

In order to prove that the proposed system is robust and unhindered by vibrations, different tests were performed using the two configurations shown in Figure 6.

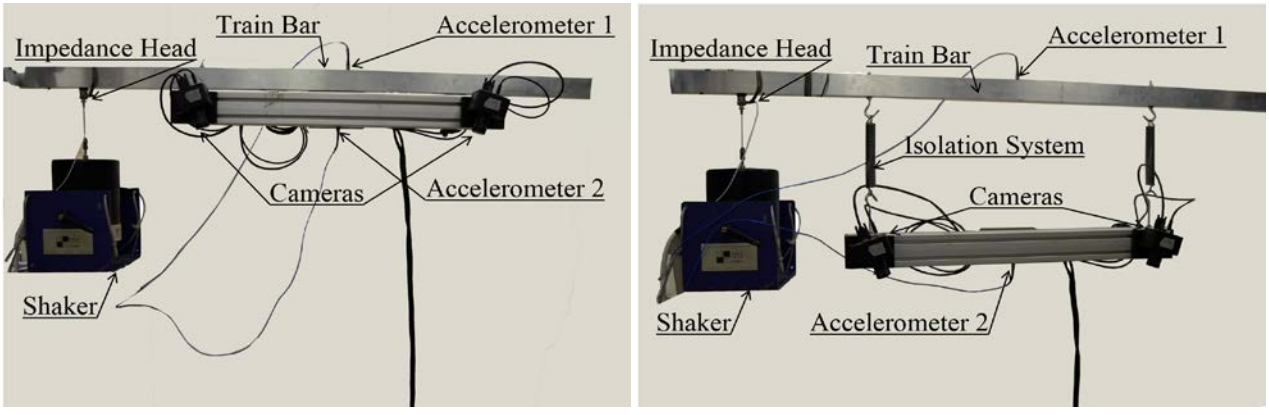

Figure 6. Experimental setup for vibration isolation assessment: hard-mounted case (left) and with isolation system installed (right).

The shaker shown in Figure 6 was used for exciting the train bar with a random noise vibration in the range 0 – 40 Hz to simulate the effect of the train motion on the cameras. An impedance head was used for measuring the input vibration's levels, while two Integrated Electronics Piezo-Electric (IEPE) sensors, Accelerometer 1 and Accelerometer 2, were used for monitoring the vibration levels on the train bar and cameras bar respectively. A portion of the time history recorded on the two bars for the two configurations analyzed are plotted in Figures 7, while Figure 8 shows the frequency responses calculated by means of a Fast Fourier Transform (FFT).

Figure 7. Detail of the time domain response: hard-mounted case (top) and with isolation system installed (bottom).

The effectiveness of the isolation system in reducing the vibration transmitted is evident. In the hard mounted case, the equivalent acceleration a_{eq} recorded on the train bar is 2.96 ms^{-2} opposed to 1.71 ms^{-2} measured on the camera bar. This equates to a reduction of nearly 42%. The accelerations recorded when the isolation system is installed are equal to 6.62 ms^{-2} and 0.25 ms^{-2} on the train bar and cameras bar respectively, showing that the springs are able to reduce the transmitted vibration by nearly 96% despite the non-optimized system. The vibration measured on the camera bar is significantly smaller than that measured in the hard-mounted case, even if the input is doubled. The witnessed reductions in vibration demonstrate the value of the isolation system. Similar considerations can be made by analyzing the computed frequency domain responses. As shown in Figure 8, the energy across the excitation frequencies is reduced by nearly 20 dB as the isolation system is installed. The only frequency that does not exhibit a significant reduction in vibration is at 2 Hz, because the natural frequency of the system is 2 Hz.

Figure 8. Detail of the frequency domain response: hard-mounted case (top) and with isolation system installed (bottom).

To validate the performance of the isolation system with regards to DIC measurements, several laboratory tests have been conducted. Tests evaluated the deflection profile of a wooden tie as it was loaded at its two free edges while the camera bar was fixed to the train bar using the two systems shown in Figure 6. A comparison of the results obtained with and without vibration was performed. One more time, an evaluation of the noise floor characteristics for the different setups has been performed (i.e. during the unloaded case), together with an evaluation of the vertical displacement Z of a longitudinal section of the tie. Table 3 summarizes the upper and lower values of the measurements' noise floor for the three analyzed conditions (absence of vibrations, hard-mounted bars with vibrations with vibrations, and isolation system installed between the two bars with vibrations).

Table 3. Measured out-of-plane displacement noise floor.

	Without vibrations	Isolated	Hard Mounted
Zmax (mm)	0.0167	0.0199	0.0386
Zmin (mm)	-0.0154	-0.0222	-0.0453
ΔZ (mm)	0.0326	0.0421	0.0839

From the data summarized in Table 3, is it possible to observe that the presence of an isolation system is effective in maintaining a noise floor consistent with that measured in the static conditions. On the other hand, for the hard mounted case the vibrations nearly triple the noise floor range. In particular, the noise floor without vibrations and with the isolated system installed ranges from $3.26 \cdot 10^{-5}$ m to $4.21 \cdot 10^{-5}$ m respectively. Both conditions are still consistent with those recorded in static conditions as shown in Table 2. Considering the hard mounted case, the noise floor is raised to $8.39 \cdot 10^{-5}$ m. As a result, strong vibrations affect the quality of the measurements and increase the value of the smallest detectable displacement, reducing the efficiency of the 3D DIC system in measuring sub-millimeter movements. A confirmation of the quality of the isolation system can be obtained when an evaluation of the tie's longitudinal profile is performed. The shape assumed by the tie is plotted for unloaded and loaded conditions for the three configurations in Figure 9. In particular, the results shown were obtained by averaging and post-processing (i.e. filtering and movement correction) the 10 images recorded for each measurement performed. For the unloaded case, the noise floor measured as the system is excited with the random vibration is higher at the two edges of the tie because of the lenses distortion effect. In these positions, no significant differences in the noise floor can be observed between the data recorded as the isolation system is installed and those measured in the hard mounted case. In the middle of the tie (i.e. where lenses distortion is less severe or absent), the profile detected when the isolation system is installed (red dots) is very close to that evaluated in static conditions (green line), while more severe differences exist when a comparison with the hard mounted case is performed (blue dots).

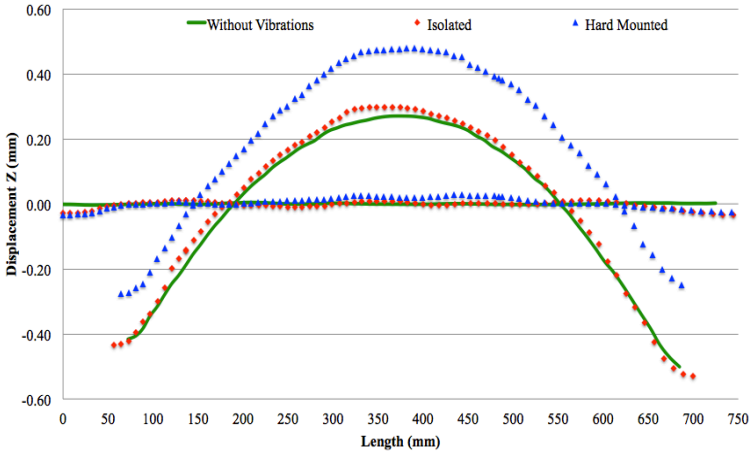

Figure 9. Tie longitudinal profiles as a function of the applied load for the three analyzed configurations.

No significant differences can be observed when the longitudinal profile measured in absence of vibration is compared to that measured with the 3D DIC system installed with the isolation system. Regarding the hard mounted case, the profile shape of the tie resembles that of the other two cases with an additional offset. The offset is likely due to the high motion of the cameras bar during the measurements and consistent with that shown in other studies, which took into account the effect of motion on the cameras [18].

3. TRACK EVALUATION USING 3D MODELS RECONSTRUCTED FROM STRUCTURE-FROM-MOTION TECHNIQUES

Another closely related approach investigated to complement the DIC system described in the previous paragraphs involves using four independent cameras and a cloud of multiple images to generate a virtual 3D rendering of the railroad track. Structure-from-Motion (SfM) is a technique that allows building a three-dimensional description of a static scene from a dense sequence of images [19]. The 3D model can then be used for performing visual inspection remotely, reducing downtime and costs associated with the investigation. In particular, once the virtual model of the object being tested has been reconstructed from the 2D images, an operator could "virtually" navigate it and detect any anomaly in the structure. If successfully developed, the images taken from cameras underneath a moving rail car could

reconstruct a 3D model of the track, which can be remotely inspected to assess crosstie integrity and to perform qualitative consideration on the health conditions of the infrastructure.

In this paragraph, an example of a 3D rendering of a railroad track obtained from a cloud of 2D images captured using a digital camera is shown. In particular, the recorded images were processed using the Pix4Dmapper image processing software released by the Swiss company Pix4D SA for obtaining a 3D virtual model. As two or more images are input in the software, Pix4Dmapper can automatically find common points, called keypoints, between those images. When two keypoints on two or more different images are found to be the same, they are matched and will generate one 3D point. As a general rule, it can be stated that the more keypoints there are, the more accurately 3D points can be computed. Therefore, the recommended overlap for most cases is equal to 75% frontal overlap and at least 60% side overlap [20]. This software, developed for large-area aerial inspections (e.g. agriculture [21, 22], geosciences [23], urbanistic [24]), can process images both with and without geolocation (i.e. Ground Control Points, GCPs). Activating a geolocation system makes it possible to locate the model from an initial an arbitrary model space to a real-world coordinate system increased the accuracy of the generated 3D rendering.

In the example presented in this research, a group of four cameras have been installed over the test article shown in Figure 1 and used for capturing a sequence of images simulating the advancement of the train along the railroad. The camera used for this experiment was a Nikon D3200, installing a zoom lens AF-S DX manufactured by Nikkor with a focal lens variable between 18 and 55 mm. Due to the camera working distance (i.e. 1 meter) and the selected focal length (i.e. 18 mm), the camera's FOV covers an area of ~0.89 x 1.30 meters. Then, assuming a camera system installed underneath the train car similar to the conceptual one showed in Figure 3 and a train speed of 27 ms^{-1} (60 mph), images should be acquired every 0.01 seconds to guarantee an overlap of 0.62 m in the direction of motion (70% of the camera's total FOV). A frame rate of 100 Hz, which is easily obtainable with the currently available cameras' technology, is required for performing this acquisition. In experiments shown in this research, only a single camera was available at the time of the tests, therefore the acquisition was simulated the advancement of the train by moving the camera by 0.27 m at each stage. Figure 10 shows a 3D SfM rendering of the mock railway tie laboratory experimental setup obtained from a total of 24 images covering a surface of 1.60 by 2.60 meter and the position of the cameras relative to the investigated object. Figure 10 also depicts a detail of the virtual rendering, showing the possibility of detecting the features of the reconstructed 3D model of the tie (e.g. the three millimeter black dots and optical target used for the DIC measurements).

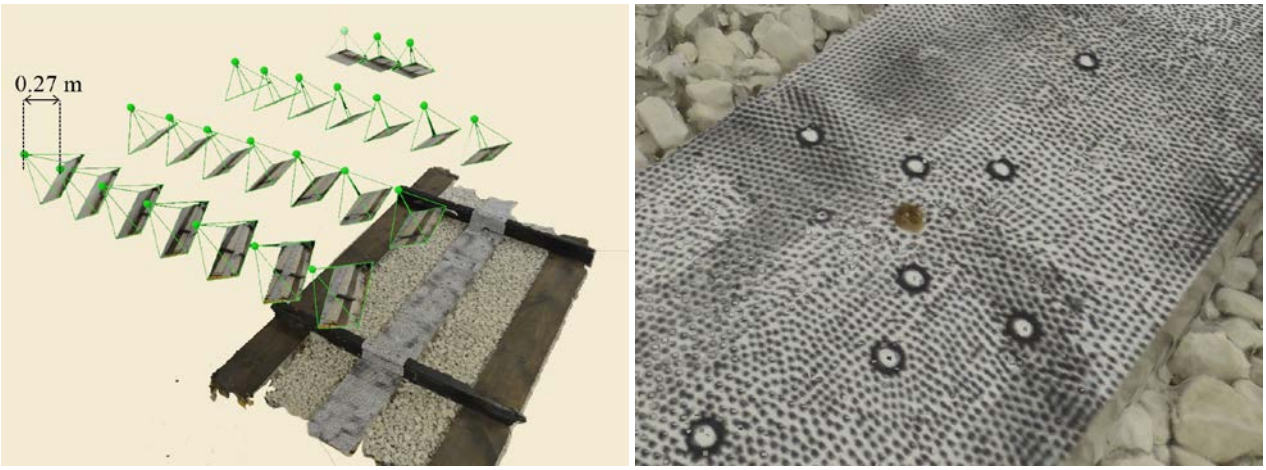

Figure 10. 3D SfM rendering of the mock railway tie laboratory experimental setup shown in Figure 1 (left) and detail of the reconstructed model starting from a cloud of 24 2D images (right).

Another example of the results that can be obtained using this technique is shown in Figure 11, showing a 3D rendering from images taken on a trolley line in Lowell, MA and details of the track itself. As observed, even the smallest features of the railroad track, such as damaged ties and fastening systems, can be clearly distinguished. From the central and rightmost images in Figure 11, it is possible to observe how the 3D model can be navigated for highlighting damage in both crossties (highlighted in yellow) and fastening systems (highlighted in red). In particular, analyzing Figure 11b is it

possible to observe that the 3D rendering can highlight the presence of both severely damaged crossties (second tie in the image) and small cracks (first tie in the image). Moreover, the same model can be used for detecting, which fastening systems are about to fail and which are still fine. On the down side, the results obtained as this technology is employed do not allow for straightforward quantitative evaluation of the structure being analyzed (e.g. displacement estimation, longitudinal profile assessment, etc.) as compared to the 3D DIC technology. This is due to the fact this technique is still in a developing stage and because all the analyses presented in this research have been performed without the support of Global Positioning System (GPS) aids to georeferencing their relative position in space. For these reasons further investigations are needed for better evaluating the Technology Readiness Level (TRL) for performing structural monitoring of civil engineering structures.

Figure 11 - 3D rendering from images on a trolley line in Lowell, MA (left), damaged crossties detail (center), fastening systems and crosstie failure (right).

4. CONCLUSIONS

In this study an integrated system for optically assessing the condition of railroad track while trains are in operation is proposed. The final goal of this research is to develop a non-contact, automated, and fast system for identifying defects or damage before they become failures. They include evaluation of the tie deflection profiles, ballast support, and investigation of the general health of the track's elements. Two complementary systems have been introduced for this purpose. The first one is a novel system based on a 3D DIC measurement technique for the measurement of tie deflection profiles and ballast support evaluation; the second employs Structure from Motion (SfM) techniques for obtaining a 3D rendering of the infrastructure from a series of two-dimensional (2D) images.

The feasibility of the proposed 3D DIC system is validated through extensive experiments performed on a full-scale railroad track model, showing the capability of the method to extract the full-field out-of-plane displacement and the longitudinal profile of the crosstie. An accuracy on the order of 10^{-4} m can be achieved with the proposed system and the possibility to characterize the differences in the crossties' deflection profiles as various ballast conditions are simulated are shown. The performed set of experiments also addresses the issue of how train vibration affects the quality of the optical measurements. Results revealed that a non-optimized isolation system is effective in reducing the vibration transmitted to the camera by nearly 96%, and even in absence of the isolation system and full vibration, the 3D DIC system is robust enough to detect the crossties' deflection profile even if some offset errors are introduced.

The second approach investigated proposes a complementary system that allows reconstructing a 3D model of the railroad, which can be virtually navigated to assess tracks' health. The results shown that this method is suitable for obtaining qualitative evaluations on the overall condition of the track from some major features, proving its efficiency in highlighting defects at a macroscopic scale (e.g. damaged crossties, missing or failing fastening systems). Due to the low accuracy of this technique and the advancement of its state-of-the-art, the SfM rendering does not allow for easily performing quantitative evaluation on the investigated infrastructure (e.g. measuring deflections, estimating displacement, etc.) yet. Nevertheless, the SfM technique is extremely promising and further investigation will be pursued to improve its function for SHM evaluations. These might include both the development of machine learning algorithms and software enhancements. Machine learning algorithms can automatically evaluate the state of the track by just processing information from pictures, avoiding the need to deploy a large array of sensors underneath the tie tested.

Software enhancements would need to increase the measurement accuracy and allow the extraction of those geometrical parameters of interest in the ballast condition assessment.

To finish, the development of both systems could increase railway safety and reduce cost for condition-based maintenance. They would represent an easy-to-use, effective, and autonomous Structural Health Monitoring (SHM) system for tie-ballast condition assessment that would allow the detection of potentially dangerous situations at an early stage and would provide an efficient way to extend the operational life of railway structures, while not interfering with train operations.

REFERENCES

[1] American Society of Civil Engineers (ASCE), "2013 Report Card for America's Infrastructure, Rail", http://www.infrastructurereportcard.org/a/#p/rail/overview (11 December 2016).

[2] Federal Railroad Administration (FRA), "2005 – 2015 Safety Statistics Data", http://safetydata.fra.dot.gov (11 December 2016).

[3] National transportation Safety Board, "Preliminary Findings Report: Mosier, Oregon; Union Pacific Derailment. 23 June 2016", http://www.transportica.info/2016/07/usdot-fra-preliminary-findings-report.html (11 December 2016).

[4] National transportation Safety Board, "Railroad Accident Brief – Metro-North Railroad Derailment. Report No. NTSB/RAB-14/11", http://www.ntsb.gov/investigations/AccidentReports/Reports/RAB1411.pdf (11 December 2016).

[5] Barke, D. and Chiu, W. K., "Structural Health Monitoring in the Railway Industry: A Review," SHM 4(1), 81-93 (2005).

[6] Buggy, S., James, S., Staines, S., et al., "Railway track component condition monitoring using optical fibre Bragg grating sensors," Meas. Sci. Technol. 27(5), 055201 (2016).

[7] Cremins, M., Shuai, Q., Xu, J., et al., "Fault detection in railway track using piezoelectric impedance," Proc. SPIE 90612 (2014).

[8] Hodge, V., O'Keefe, S., Weeks, M., et al., "Wireless Sensor Networks for Condition Monitoring in the Railway Industry: A Survey," IEEE Trans Intell. Transport Syst. 16(3), 1088-1106 (2015).

[9] Greene, R., Yates, J. A. and Patterson, E. A., "Crack detection in rail using infrared methods," Opt. Eng. 46(5), 051013 (2007).

[10] Lanza di Scalea, F. [Ultrasonic Testing Applications in the Railroad Industry], American Society for Nondestructive Testing, Columbus, 535-540 (2007).

[11] Olhoeft, G. R. and Selig, E. T., "Ground-penetrating radar evaluation of railway track substructure conditions," Proc. 9th International Conference GPR2002, 48-53 (2002).

[12] Koenderink, J. J. and Van Doorn, A. J., "Affine structure from motion". JOSA A. 8(2), 377-385 (1991).

[13] LeBlanc, B., Niezrecki, C., Avitabile, P., et al., "Damage detection and full surface characterization of a wind turbine blade using three-dimensional digital image correlation," *SHM* 12(5-6), 430-439 (2013).

[14] Yu, H., "Estimating Deterioration in the Concrete Tie-Ballast Interface Based on Vertical Tie Deflection Profile: A Numerical Study,". Proc. Joint Rail Conference, V001T01A024 (2016).

[15] Poozesh, P., Baqersad, J., Niezrecki, C., Avitabile, P., Harvey, E. and Yarala, R., "Large-area photogrammetry based testing of wind turbine blades," Mech. Syst. and Sign. Proc 86(B), 98-115 (2017).

[16] Schmidt, T., Tyson, J., Galanulis, K., "Full-Field Dynamic Displacement and Strain Measurement Using Advanced 3D Image Correlation Photogrammetry: Part I," Exp Tech. 27(3), 47-50 (2003).

[17] Schmidt, T., Tyson, J., Galanulis, K., "Full-Field Dynamic Displacement and Strain Measurement Using Advanced 3D Image Correlation Photogrammetry: Part II," Exp Tech. 27(4), 22-26 (2003).

[18] Balcaen, R., Reui, P.L., Lava, P. et al., "Evaluation of Camera Motion in Stereo-DIC," Proc. iDICs 2016, in press.

[19] Bolles, R. C., Baker, H. H., and Marimont, D. H., "Epipolar-plane image analysis: An approach to determining structure from motion," International Journal of Computer Vision 1(1), 7-55 (1987).

[20] Pix4D, "Offline Getting Started and Manual", https://support.pix4d.com/hc/en-us/articles/204272989-Offline-Getting-Started-and-Manual-pdf-#gsc.tab=0 (11 December 2016).

[21] Turner, D., Lucieer, A., and Watson, C. "An automated technique for generating georectified mosaics from ultra-high resolution unmanned aerial vehicle (UAV) imagery, based on structure from motion (SfM) point clouds,". Remote Sensing 4(5), 1392-1410 (2012).

[22] Jay, S., Rabatel, G., Hadoux, X., Moura, D., and Gorretta, N., “In-field crop row phenotyping from 3D modeling performed using Structure from Motion,” Computers and Electronics in Agriculture 110, 70-77 (2015).
[23] Westoby, M. J., Brasington, J., Glasser, N. F., Hambrey, M. J., and Reynolds, J. M., “Structure-from-Motion’photogrammetry: A low-cost, effective tool for geoscience applications,” Geomorphology 179, 300-314 (2012).
[24] Pollefeys, M., Nistér, D., Frahm, J. M., Akbarzadeh, A., Mordohai, P., et al., “Detailed real-time urban 3d reconstruction from video,” International Journal of Computer Vision 78(2-3), 143-167 (2008).